44th AIAA/ASME/ASCE/AHS Structures, Structural Dynamics, and Materials Confere
7-10 April 2003, Norfolk, Virginia

AIAA 2003-1487

NONLINEAR AEROELASTIC ANALYSIS OF JOINED-WING AIRCRAFT

Mayuresh J. Patil*
Widener University, Chester, PA 19013-5792

Joined-wing aircraft are being designed for 'sensorcraft' configuration. Joined wings lead to multiple load paths and constraints. The focus of this work is to understand the nonlinear structural as well as aeroelastic behavior of joined wings. The paper presents a formulation for the nonlinear aeroelastic analysis of joined wings. Results are presented for two joined wings configurations. Overall, the joined wings are found to be stiffer than single wing configuration. The 'non-planar' joined wing is found to be stiffer than the 'planar' joined wing. The structural dynamic characteristics of the joined wings are also presented. The bending modes are similar to the cantilevered beam modes while the torsional vibrations are restricted to the unconstrained part of the main wing. The structural analysis showed negligible nonlinear effects for static deformation as well as for structural dynamics characteristics.

Introduction

In recent years there has been a push towards the design and development of uninhabited aerial vehicles (UAVs). UAVs are being designed for various missions including atmospheric sensing, border monitoring, military reconnaissance and combat (UCAV). It is expected that UAVs would not only take over multiple conventional roles in civilian as well as military service, but also undertake new unconventional missions in the future.

One example of an unconventional a mission is the 'sensorcraft.' Sensorcraft is being designed for long-range, high-altitude, intelligence, surveillance and reconnaissance (ISR). Sensorcraft is a joined-wing design aimed at providing an unobstructed field of view around the vehicle.[1] Weisshaar and Lee[2] present the history of joined-wing aircraft. The paper also presents aeroelastic tailoring studies. Livne[3] presents a literature survey of the present status of technical development.

Aeroelastic stability and response are critical in the design of joined-wing aircraft. Joined-wing aircraft differ considerably from conventional aircraft. The wings are expected to be long and flexible leading to high deformation. Analysis of such wings may require geometrically nonlinear structural and aerodynamic analysis. The constraints imposed by the joint are likely to impose stress concentration. Additional buckling-like nonlinearity have also been reported.[4] Analysis of joint mechanisms and its effect on the structure (local and global) is essential. Linear, cantilevered wing analysis tools, which are routinely used for conventional wings, cannot be used to analyze joined wings. The aeroelastic analysis and design of such joined-wing aircraft is the topic of this paper.

*Assistant Professor, Department of Mechanical Engineering. Member AIAA.

Present Work

A nonlinear aeroelastic analysis methodology has been developed and is being implemented. The analysis is centered around a geometrically exact structural model for the dynamics of beam-like structures.[5] This analysis accounts for large deformation of the wing and fuselage. The analysis has been coupled with various aerodynamic models to investigate the nonlinear aeroelastic behavior and flight dynamics of High Altitude, Long Endurance (HALE) aircraft.[6,7] Joint constraint equations are added to the nonlinear structural formulation. The structural analysis is then coupled with an unsteady, vortex-lattice aerodynamic model.[8]

Theory

The structural formulation used in the present research is based on the mixed variational formulation for dynamics of moving beams.[5] Equations of motion are generated by including the appropriate energies in a variational principle followed by application of calculus of variation. The final equations are presented here.

By using simple shape functions, the mixed variational formulation leads to a set of coupled nonlinear differential equations in terms of the element nodal displacements (u) and rotations (θ), nodal internal forces (F) and moments (M), and linear and angular velocities (V and Ω). Rodrigues parameters are used as rotational variables (θ). The equations presented below are all vector equations for each finite element in the structural representation. The equations have been simplified and do not include the nonlinear terms arising from the kinetic energy (in terms of the velocities), because the only problems that are of interest in the present work are nonlinear static equilibrium and dynamic small perturbation analysis. The equations for the n^{th} element can be

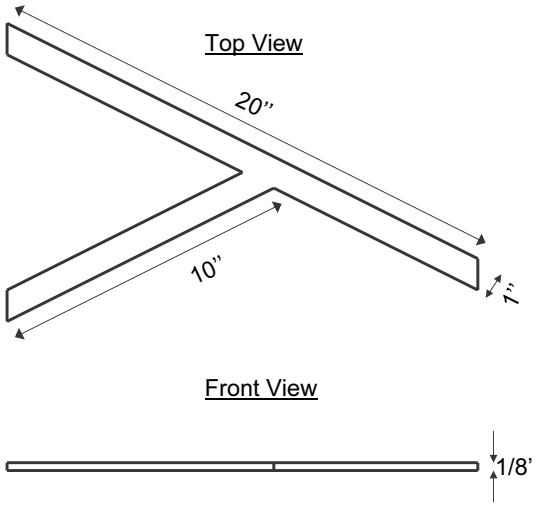

Fig. 1 Planar joined-wing configuration

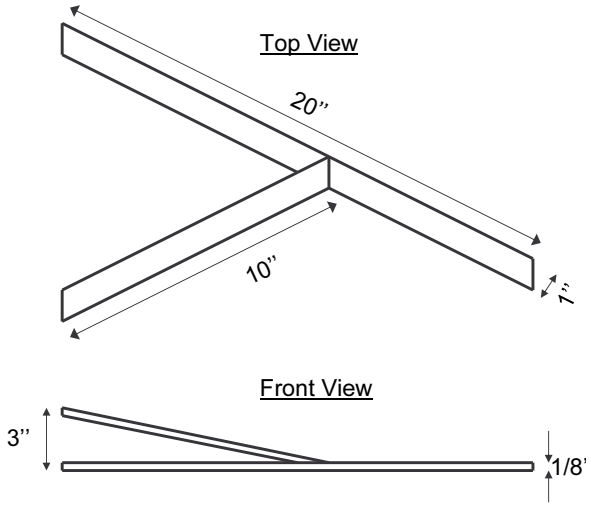

Fig. 2 Non-planar joined-wing configuration

written as

$$\begin{gathered}
\frac{F^{n+1}-F^n}{\Delta\ell} + f_{aero} + \widetilde{\overline{\kappa}}^n(\frac{F^n+F^{n+1}}{2}) - \dot{\overline{P}}^n = 0 \\
\frac{M^{n+1}-M^n}{\Delta\ell} + m_{aero} + (\widetilde{e}_1 + \widetilde{\overline{\gamma}}^n)(\frac{F^n+F^{n+1}}{2}) \\
+\widetilde{\overline{\kappa}}^n(\frac{M^n+M^{n+1}}{2}) - \dot{\overline{H}}^n = 0 \\
\frac{u^{n+1}-u^n}{\Delta\ell} + e_1 - C^{is}(\overline{\gamma}^n + e_1) = 0 \\
\frac{\theta^{n+1}-\theta^n}{\Delta\ell} - (I + \frac{\tilde{\overline{\theta}}^n}{2} + \frac{\overline{\theta}^n(\overline{\theta}^n)^T}{4})\overline{\kappa}^n = 0 \\
\dot{u}^n - C^{is}V^n = 0 \\
\dot{\theta}^n - (I + \frac{\tilde{\theta}^n}{2} + \frac{\theta^n(\theta^n)^T}{4})\Omega^n = 0
\end{gathered} \tag{1}$$

where $\overline{\gamma}$ and $\overline{\kappa}$, the strains and curvatures, are related to F and M via a cross-sectional constitutive law, and $\overline{P}$ and $\overline{H}$, the linear and angular momenta, are related to V and Ω using the cross-sectional inertial properties, as

$$\begin{Bmatrix} \overline{\gamma} \\ \overline{\kappa} \end{Bmatrix} = [\mathcal{S}] \begin{Bmatrix} \frac{F^n+F^{n+1}}{2} \\ \frac{M^n+M^{n+1}}{2} \end{Bmatrix} \tag{2}$$

$$\begin{Bmatrix} \overline{P} \\ \overline{H} \end{Bmatrix} = [\mathcal{I}] \begin{Bmatrix} \frac{V^n+V^{n+1}}{2} \\ \frac{\Omega^n+\Omega^{n+1}}{2} \end{Bmatrix} \tag{3}$$

The direction cosine matrix C^{is} transforms the components of a vector from the s-frame corresponding to the deformed structure to i-frame corresponding to the undeformed straight wing. The direction cosine can be written in terms of the Rodrigues parameters as

$$C^{is} = \frac{(1 - \frac{\theta^T\theta}{4})\Delta + \tilde{\theta} + \frac{\theta\theta^T}{2}}{1 + \frac{\theta^T\theta}{4}} \tag{4}$$

f_{aero} and m_{aero} are the aerodynamic forces and moments acting on each element, and are calculated using aerodynamic theory described below.

The aerodynamic analysis methodology is based on an unsteady vortex lattice method.[8] In unsteady vortex lattice method, vortices are distributed on the wing as well as in the wake. Various conditions on the vortex strengths are then imposed to solve the problem dynamically. The discrete unsteady vortex lattice relations are summarized below.

a) Vorticity-downwash relation relate the downwash at the control points on the wing (due to structural deflections) to the downwash induced by bound and wake vorticity, as

$$K_b{\Gamma_b}^{n+\frac{1}{2}} + K_w{\Gamma_w}^{n+\frac{1}{2}} - W^{n+\frac{1}{2}} = 0 \tag{5}$$

where, Γ_b and Γ_w denote the bound and wake vortices, K_b and K_w are the corresponding induced velocity coefficients, W denotes the downwash due to structural deflections, and the superscript denotes the time iteration at which the variable are calculated.

b) Shed vorticity - bound vorticity relation relates the change in bound vorticity to the wake vorticity shed in that time interval.

$$\Sigma{\Gamma_b}^n - \Sigma{\Gamma_b}^{n+1} - {\Gamma_{w_1}}^{n+1} = 0 \tag{6}$$

c) Convection of shed vorticity relation state that at each iteration the vorticity travel at the airspeed to the next vortex element.

$${\Gamma_{w_{i+1}}}^{n+1} - {\Gamma_{w_i}}^n = 0 \tag{7}$$

The lift is now given by

$$L = \rho U\Gamma_b + \rho b\dot{\Gamma}_b \tag{8}$$

Coupling the structural equations with the aerodynamic equations, one can obtain the complete nonlinear aeroelastic equations of motion. These equations can be solved using the iterative Newton-Raphson method to determine the trim state. The nonlinear aeroelastic system is then linearized about the trim state. The stability of the trim state can be ascertained by solving the eigenvalue problem of the linearized aeroelastic system.

Results

Two joined-wing configurations are selected for analyses. Both the configurations have a swept main wing and a rear wing connected to the main wing at the main wing mid-span. The wings are made of 1 in by 1/8 in aluminum bars. The length of the main wing is 20 in. The 'planar wing' is shown in Fig. 1. Here the main wing and the rear wing are in the same plane. The 'non-planar wing' is shown in Fig. 2. Here the root of the rear wing is offset 3 in from the root of the main wing. Thus the rear wing is angled downward from the root to the tip. A non-planar configuration may be aerodynamically more efficient due to reduced aerodynamic interference.

The wings described above were manufactured and tested by applying a tip load. The experimental setup is described in detail in [9]. The analysis described in the paper was used to solve the static structural analysis problem.

Static Structural Solution

Fig. 3 shows the load versus deformation curves for the planar wing. Fig. 3(a) shows the vertical deflection at the joint due to the applied tip load. The figure plots the experimental data points, analysis results from the complete nonlinear solution as well as the results obtained using linear approximation. The analysis results and the experimental data are quite close. Also, linear analysis is sufficient to characterize the structural deformation of the wing.

Fig. 3(b) presents the deflection at the tip due to the load at the tip for the planar wing. The theoretical and experimental solutions are in close agreement for tip loads below 3 lbs. Above 3 lbs the experimental deflection increase more rapidly than the theoretical solution. This is due to yielding at the joint. Again, the linear approximation gives reliable results.

Fig. 4 shows the joint as well as tip deflection due to applied tip load for the non-planar wing. The theoretical predictions for the joint deflections are lower than that observed experimentally. This difference can be attributed to the inability of a beam model to accurately represent the exact joint boundary conditions. The theoretical tip deflections are in agreement with the experimental data for loads below 3 lbs. Again, above 3 lbs, the experimental wing started to yield near the joint. Also, the linear approximation is quite good.

Table 1 Comparison of wing deflections

Configuration	Joint Defl. (in)	Tip Defl. (in)
Single (main) wing	1.954	5.459
Joined-wing (planar)	0.894	2.656
Joined-wing (non-planar)	0.143	0.828

The next case study used a distributed load instead of a concentrated load. The distributed load represents the distributed lift on the wing. Load intensity of 0.5 lbs/in is selected. The stresses due to this load are below the yield point of the material. Fig. 5 shows the deflection of the planar wing under the distributed load. Fig. 6 shows the deflection of the non-planar wing for the same distributed load. The deflection of the non-planar wing is much lower than that of the planar wing. Table 1 presents the tip and joint deflections due to the distributed load. The rear wing stiffens the main wing considerable. The deflections of the planar wing is less than half that calculated for a single wing with the same loading. The non-planar wing is even stiffer than the planar wing. The out-of-plane rear wings leads to a stronger constraint on the main wing. The tip deflection of the non-planar wing is one-third that of the deflection for planar wing.

The rear wing, especially in the non-planar case carries some compressive load and is thus able to constrain the vertical motion of the main wing at the joint. The compressive load can lead to buckling of the rear wing. The likelihood of buckling increases with decrease in the rear wing thickness. To study the possibility of buckling, structural analysis is conducted by varying thickness. Fig. 7 shows the non-planar wing deflection for varying rear-wing thickness. As the thickness of the rear wing is reduced, there is increase in the rear wing deformation, and a reduction in the constraint force, leading to higher deformation of the main wing. For rear-wing thickness of 0.025 in, one-fifth the nominal thickness, the rear wing starts showing buckling-like deformation. For lower rear-wing thickness, the Newton-Raphson method failed to converge.

Structural Dynamic Analysis

Structural dynamic analysis is conducted on the joint wing. Fig. 8 shows the three modes of the planar wing. The first two modes are the 1^{st} and 2^{nd} bending modes. The first bending mode is similar to that of a cantilevered beam. The second bending mode also vibrates like the second cantilevered beam bending

Table 2 Effect of load on the frequencies

Mode	Frequency without load (rad/s)	Frequency with load (rad/s)
planar wing		
1^{st} bend. mode	4.974	5.094
2^{nd} bend. mode	19.87	20.11
1^{st} tors. mode	169.9	172.5
non-planar wing		
1^{st} bend. mode	8.768	8.726
2^{nd} bend. mode	24.84	24.77
1^{st} tors. mode	225.8	225.7

mode. The torsional mode vibration on the other hand is dominant only on the main wing between the joint and the tip. The joint constrains the torsional vibrations so that the main as well as the rear wing between the root and the joint cannot twist. Thus the torsional frequency is very high and similar to that of a cantilevered beam starting at the joint.

Fig. 9 shows the three modes of vibration for the non-planar wing. The first bending mode seems to be constrained at the joint and thus the first bending frequency for the non-planar wing is much higher than the planar wing. The second bending mode on the other hand shows some deflection at the joint and thus its frequency is close to the planar wing frequency. Finally, the torsional mode is similar to the planar wing mode. The joint again constrains any twist and the dominant motion is seen between the joint and the tip of the main wing.

Finally, it has been shown that non-trivial steady state, including large deformations and internal forces, can lead to significant change in the structural dynamic characteristics of the wing.[10] Table 2 shows the frequencies for the planar and non-planar wings, without and with applied load. The frequencies do not change much with applied load. The mode shapes for a loaded wing are also quite similar to the mode shapes for the unloaded wing.

Conclusions

A methodology for the nonlinear aeroelastic analysis of joint wings has been developed. The analysis takes into account geometrical nonlinearities of the structure as well as the flow. The methodology for the structural dynamic analysis was implemented in Matlab. Two test case joined-wings were used to test the analysis methodology. The theoretical results were in good agreement with the experimental results. The nonlinear analysis results were close to the linear analysis results. The joined wings were shown to be much stiffer than a similar single wing. The non-planar joined wing was shown to be stiffer than the planar joined wing. Structural dynamic analysis of joined wings indicates that the joined wings have higher frequencies (as compared to single wing) because of the constraints imposed by the joint. The joint leads to the torsional mode being exhibited only on the main wing between the joint and the tip. Finally, there was no significant effect of the load on the structural dynamic characteristics of the wing. Thus, the structural nonlinearities were quite negligible.

References

[1] Ackerman, R. K., "Air Force Researchers Set Stratospheric Goals," SIGNAL: AFCEA's Journal for Communications, Electronics, Intelligence, and Information Systems Professionals, Feb. 2001.

[2] Weisshaar, T. and Lee, D., "Aeroelastic Tailoring of Joined-Wing Configurations," *Proceedings of the 43rd Structures, Structural Dynamics and Materials Conference*, Denver, Colorado, April 2002, AIAA-2002-1207.

[3] Livne, E., "Aeroelasticity of joined-wing airplane configurations - Past work and future challenges - a survey," *Proceedings of the 42nd Structures,Structural Dynamics and Materials Conference*, Seattle, Washington, April 2001, AIAA-2001-1370.

[4] Blair, M. and Canfield, R., "A Joined- Wing Structural Weight Modeling Study," *Proceedings of the 43rd Structures,Structural Dynamics and Materials Conference*, Denver, Colorado, April 2002, AIAA-2002-1337.

[5] Hodges, D. H., "A Mixed Variational Formulation Based on Exact Intrinsic Equations for Dynamics of Moving Beams," *International Journal of Solids and Structures*, Vol. 26, No. 11, 1990, pp. 1253 – 1273.

[6] Patil, M. J., Hodges, D. H., and Cesnik, C. E. S., "Nonlinear Aeroelasticity and Flight Dynamics of High-Altitude Long-Endurance Aircraft," *Journal of Aircraft*, Vol. 38, No. 1, Jan. – Feb. 2001, pp. 88 – 94.

[7] Patil, M. J., Hodges, D. H., and Cesnik, C. E. S., "Limit Cycle Oscillations in High-Aspect-Ratio Wings," *Journal of Fluids and Structures*, Vol. 15, No. 1, Jan. 2001, pp. 107 – 132.

[8] Hall, K. C., "Eigenanalysis of Unsteady Flows About Airfoils, Cascades, and Wings," *AIAA Journal*, Vol. 32, No. 12, December 1994, pp. 2426–2432.

[9] Dreibelbis, B. and Barth, J., "Structural Analysis of Joint Wings," *AIAA Midatlantic Regional Student Conference*, College Park, Maryland, April 2003.

[10] Patil, M. J. and Hodges, D. H., "On the Importance of Aerodynamic and Structural Geometrical Nonlinearities on Aeroelastic Behavior of High-Aspect-Ratio Wings," *Proceedings of the 41st Structures, Structural Dynamics and Materials Conference*, Atlanta, Georgia, April 2000, AIAA-2000-1448.

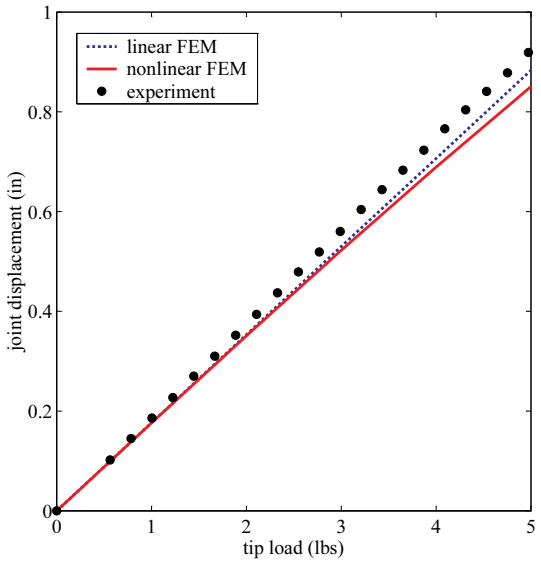

a) Joint deflection

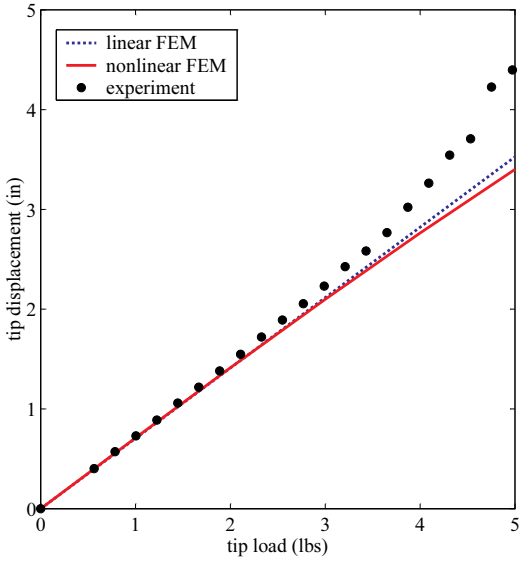

b) Tip deflection

Fig. 3 Load versus deflection curves for the planar wing

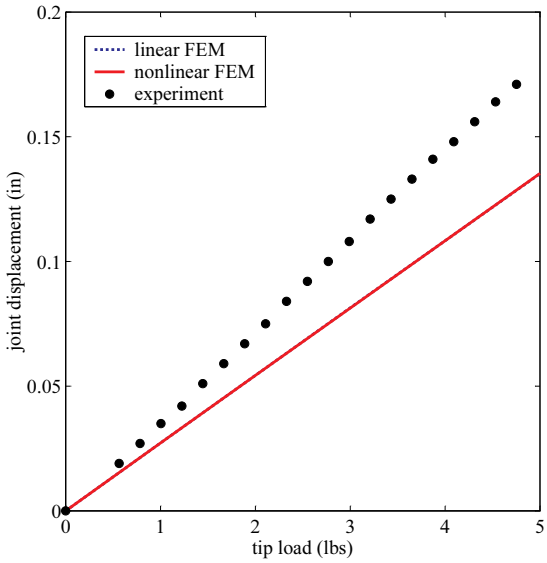

a) Joint deflection

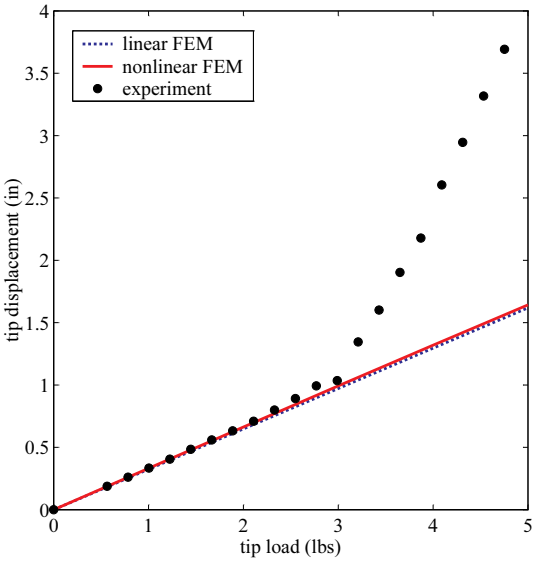

b) Tip deflection

Fig. 4 Load versus deflection curves for the nonplanar wing

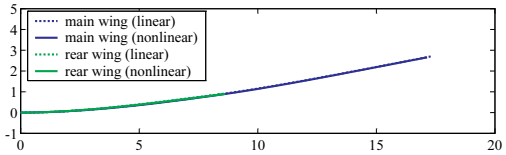

a) Beam bending deflection

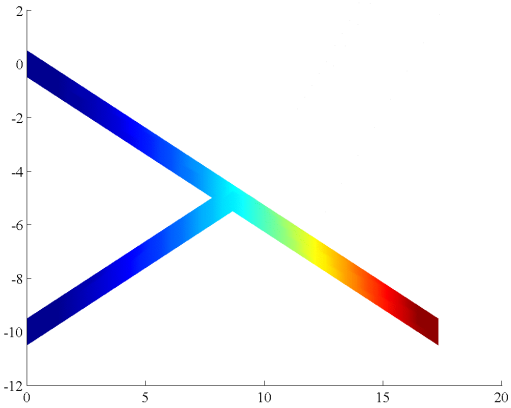

b) Deflection contours

Fig. 5 Wing deflection of planar wing due to distributed load

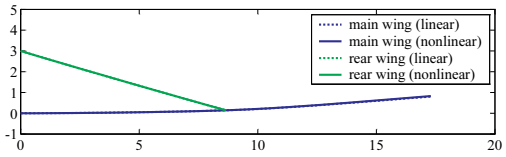

a) Beam bending deflection

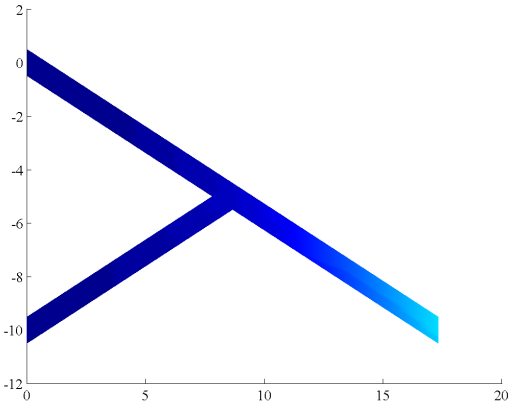

b) Deflection contours

Fig. 6 Wing deflection of non-planar wing due to distributed load

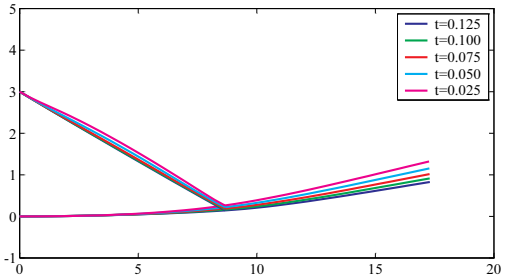

Fig. 7 Effect of rear wing thickness on the deformation of the main wing

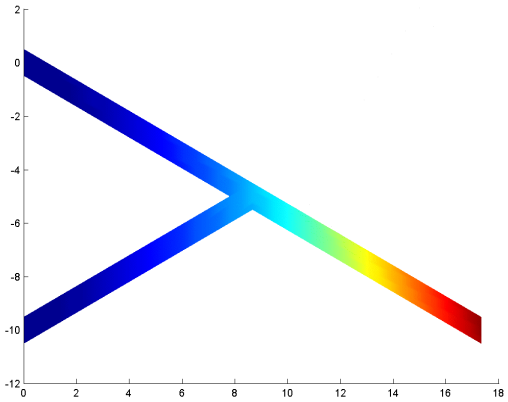

a) 1^{st} bending mode (4.97 rad/s)

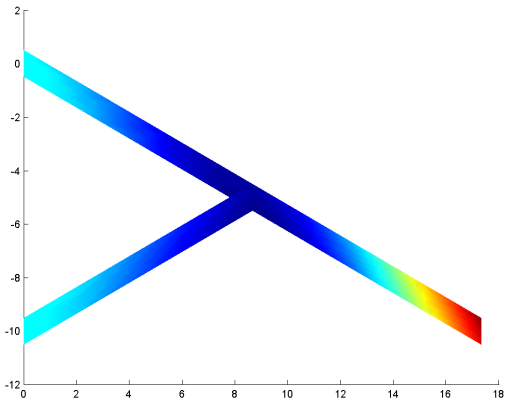

b) 2^{nd} bending mode (19.9 rad/s)

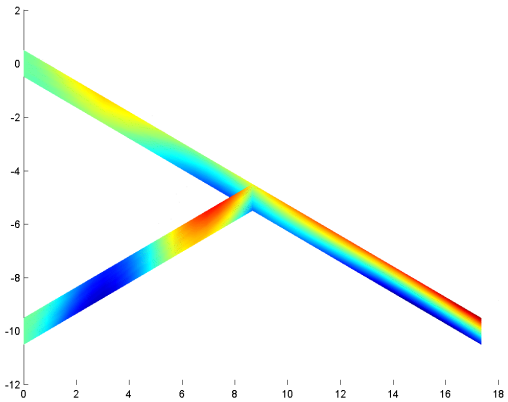

c) 1^{st} torion mode (170 rad/s)

Fig. 8 Mode shapes for the planar wing

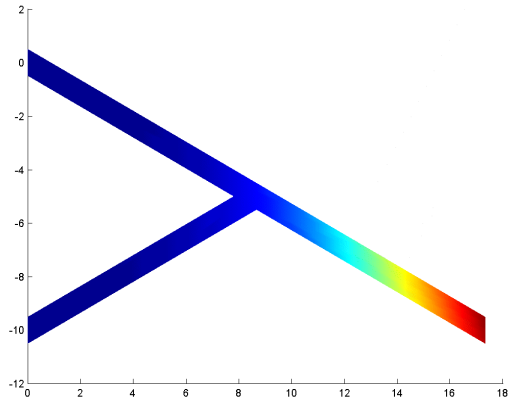

a) 1^{st} bending mode (8.77 rad/s)

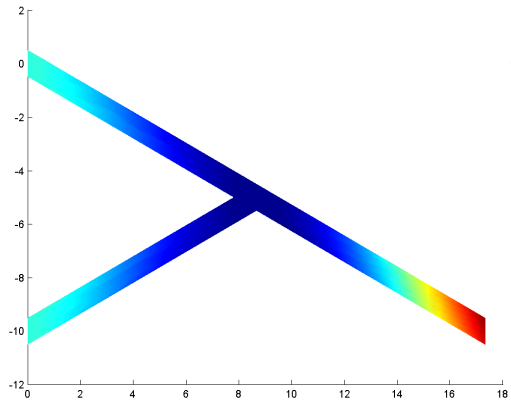

b) 2^{nd} bending mode (24.8 rad/s)

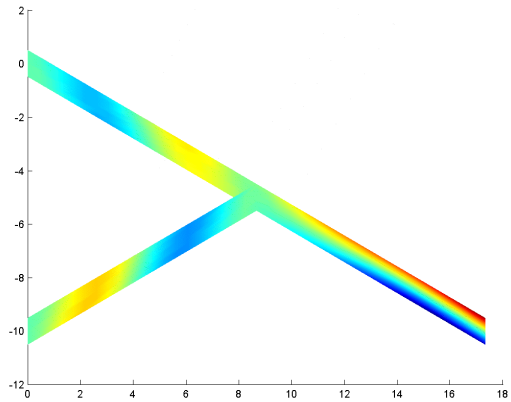

c) 1^{st} torion mode (226 rad/s)

Fig. 9 Mode shapes for the non-planar wing